

# Interface-Driven Growth Mode Control of 2D GaSe on 3D GaAs Substrates with Distinct Crystallographic Orientations

Aida Sheibani<sup>\*,1</sup>, Mohammad Zamani<sup>2</sup>, Charles Paillard<sup>1,2,3</sup>, Kanagaraj Moorthi<sup>2</sup>, Fernando Maia de Oliveira<sup>2</sup>, Serhii Kryvyi<sup>2</sup>, Mourad Benamara<sup>2</sup>, Hryhorii Stanchu<sup>2</sup>, Calbi Gunder<sup>4</sup>, Hugh Churchill<sup>1,2</sup>, Yuriy I. Mazur<sup>2</sup>, and Gregory Salamo<sup>†1,2</sup>

<sup>1</sup>*Smart Ferroic Materials center, Physics Department, University of Arkansas, Fayetteville, AR 72701, USA.*

<sup>2</sup>*Institute for Nanoscience and Engineering, University of Arkansas, Fayetteville, AR 72701, USA.*

<sup>3</sup>*Université Paris-Saclay, CentraleSupélec, CNRS, Laboratoire SPMS, 91190, Gif-sur-Yvette, France.*

<sup>4</sup>*Air Force Research Laboratory, 2241 Avionics Circle, Wright-Patterson AFB, OH 45433, USA.*

## ABSTRACT

Previous studies of the growth of two-dimensional (2D) gallium selenide (GaSe) by molecular beam epitaxy (MBE) on a gallium arsenide (GaAs) three-dimensional (3D) substrate have reported significant differences in growth morphology, polytype, and the nature of the interface. The results differ, ranging from GaSe 2D film growth at tilted 2D planes to observed spiral structures, thereby calling for a deeper understanding of the impact of the substrate interface on the growth of GaSe films. In this paper, we conduct a comprehensive reexamination of the growth mechanism of GaSe on GaAs substrates with (211)B and (001)B orientations, investigating the nature of the 2D/3D interface and the resulting morphology of the 2D GaSe films. We do this by investigating different methods of preparation of the GaAs substrate surface before the growth of GaSe by MBE, the importance of which has not been considered before. Our results resolve the mechanistic origin of tilted versus non-tilted 2D growth and establish a general interface-driven orientation selection rule linking substrate symmetry and dangling-bond coordination to layered heteroepitaxy. This framework provides a scalable interface-engineering pathway for deterministic

control of layered chalcogenide heterostructures and enables wafer-scale integration with established semiconductor device platforms.

Corresponding author:

\*asheiban@uark.edu

Keywords: Gallium selenide, Molecular beam epitaxy, Van der Waals, 2D materials.

## 1. Introduction

Of the many possible two-dimensional (2D) materials, gallium selenide (GaSe) is of interest due to a direct band gap producing photoluminescence at  $\sim 2$  eV which can potentially be tuned through thickness control or strain engineering for optoelectronic applications<sup>1, 2, 3</sup>. Moreover, GaSe 2D layers lack inversion symmetry and consequently enable second-order nonlinear optical properties<sup>4-6</sup>. The GaSe layered structure consists of Se-Ga-Ga-Se units bonded via strong in-plane covalent bonds and stacked along the out-of-plane direction through weak van der Waals forces that allow for exfoliation. Unfortunately, the Ga-Ga bonding is weaker than Ga-Se resulting in challenges for exfoliation<sup>7</sup>. For example, although GaSe can be exfoliated from bulk crystals, it often yields films with irregular size and quality<sup>8, 9</sup>. In contrast, direct deposition of GaSe films by molecular beam epitaxy (MBE) has potential for precise thickness control, uniform coverage, and high quality<sup>10</sup>. However, in this case, the choice of substrate plays a critical role in determining the growth mode, structural quality, and interfacial bonding<sup>11</sup>. Ideally, 2D GaSe films could potentially grow on a substrate without bonding to it. Although 2D materials can potentially act as a non-bonding van der Waals substrate, their limited size and availability limit their use as an MBE substrate. As a result, three-dimensional (3D) substrates like gallium arsenide (GaAs), silicon (Si), and indium arsenide (InAs) have been investigated as a substrate to grow GaSe<sup>12</sup>. For example, Kojima et al.<sup>13</sup> investigated the epitaxial growth of GaSe on GaAs substrates with (001), (111), and (112) orientations and reported GaSe 2D film growth from the surface at tilted angles. Similarly, Sorokin et al.<sup>14</sup> also conducted a study of GaSe growth on GaAs(001) and GaAs(211), but do not confirm tilted growth at the angles observed by Kojima et al.<sup>13</sup> Likewise, Diep et al.<sup>15</sup> investigated GaSe grown on GaAs(001) and observed spiral structures but without tilted growth. While all three investigated the growth of GaSe on GaAs there are significant

differences in reported observations. The variability in reported observations calls for a comprehensive investigation of key control parameters which govern the morphology of a 2D material such as GaSe on a 3D surface.

In this paper, we further examine the role of the 3D substrate on the nature of the 2D/3D interface and the morphology of 2D growth. We do this by investigating different methods of preparation of the GaAs substrate surface before the growth of GaSe by MBE, the importance of which has not been considered before. More specifically, through a combination of in-situ reflection high-energy electron diffraction (RHEED), X-ray diffraction (XRD), atomic force microscopy (AFM), transmission electron microscopy (TEM), Raman spectroscopy, and photoluminescence (PL) measurements, we systematically examine the impact of: *(i)* oxide removal *(ii)* surface preparation with Se, *(iii)* adding a GaAs buffer layer, and *(iv)* non-oxide removal before the growth of GaSe by MBE on GaAs substrates with (001)B, and (211)B orientations. Our results reveal how substrate preparation and subsequent bonding of the GaSe film with the substrate explain the different outcomes reported in previous studies and add insight on the mechanism for growth of a 2D material on a 3D substrate.

## 2. Experimental Methods

A Riber-32 MBE system equipped with Se and Ga Knudsen effusion cells and an in-situ RHEED system was used to study the growth mechanisms and interface of GaSe films on GaAs substrates. Epi-ready GaAs(B) substrates (Wafer Tech) with (211)B and (001)B orientations were prepared prior to growth. The substrates were solvent-cleaned in acetone and methanol following standard GaAs procedures<sup>16</sup>, mounted on a molybdenum holder, and loaded into a load-lock chamber, where they were heated at 200°C for 1 hour to remove residual water. The substrates were then transferred to a vacuum degas chamber and thermally cleaned at 350°C for 2 hours. For

the current investigation, these prepared epi-ready GaAs(211)B and GaAs(001)B substrates were each divided into four sets before experiments on the growth of GaSe:

***Set 1: Oxide Removed*** - The oxide was thermally removed by introducing the substrate inside the chamber and increasing the temperature into the oxide desorption window (580-620 °C) depending on the substrate orientation, without introducing Se or As flux, and the process was monitored via RHEED intensity. Following oxide removal, rather blurry RHEED reconstruction streaks are observed, indicating a rough GaAs Ga-terminated surface.

***Set 2: Oxide Removed under Se Flux*** - Substrates were ramped from 60°C to 350°C at a rate of 10°C/min, after which Se flux was introduced. The substrate temperature was then ramped further into the oxide desorption window (580-620 °C) at which time the RHEED intensity rose and plateaued indicating complete oxide desorption in a Se environment. To ensure complete oxide desorption, the substrates were held at this temperature for 10 min before cooling to the GaSe growth temperature. Prior to initiating GaSe growth on the prepared GaAs substrates, streaky RHEED patterns were obtained with Kikuchi line patterns by maintaining Se flux aiming to create a Se-terminated GaSe surface.

***Set 3: Oxide Removed and GaAs Buffer Added*** - Substrates were transferred to the III-V chamber and ramped in temperature to the oxide desorption window (580-620 °C), but with an As flux supplied during oxide removal. RHEED monitoring confirmed desorption, after which the temperature was held at the desorption point for 10 min before cooling to a GaAs buffer growth temperature, which was around 580°C. A GaAs buffer layer was then grown following the procedure of Wangila et al<sup>17</sup>.

***Set 4: Oxide Not Removed*** - Native oxide layer remained on the substrate surface and used for direct growth of GaSe on an oxide surface.

Each of these eight GaAs(211)B and GaAs(001)B prepared substrates were then used to grow GaSe under the same growth conditions to examine the role of the surface preparation on the growth morphology and the corresponding nature of the interface.

The beam-equivalent pressures (BEP) were  $\text{Ga} = 0.71 \times 10^{-7}$  Torr and  $\text{Se} = 3.5 \times 10^{-7}$  Torr, giving  $\text{Se:Ga} \approx 5:1$ . The effusion cell temperatures were  $T_{\text{Ga}} = 850^\circ\text{C}$  and  $T_{\text{Se}} = 150^\circ\text{C}$ . Growth was initiated by opening both shutters of Ga and Se cells at the same time at the growth temperature  $T_g = 400^\circ\text{C}$  and proceeded for 60 min for all the samples. For set 3, to suppress As desorption from the surface, we first deposited GaSe for 60 s at  $T_g = 375^\circ\text{C}$ , and then increased to  $400^\circ\text{C}$  for further growth of GaSe for 60 minutes.

Surface roughness and morphology of the samples were assessed using a Bruker D3100 AFM system (tapping mode, HQ.NSC15/Al BS tips, MikroMasch). XRD measurements were performed using a PANalytical X’Pert MRD system (PANalytical, Almelo, Netherlands) equipped with a 1.6 kW Cu  $\text{K}\alpha_1$  x-ray source ( $\lambda = 1.540598 \text{ \AA}$ ) with a vertical line focus, a symmetric  $4 \times \text{Ge}(220)$  monochromator, and a Pixel detector. Raman and photoluminescence (PL) characterization equipment consisted of a Horiba Jobin-Yvon LabRam HR spectrometer, equipped with a Si charge-coupled device detector and a microscope system with a 100x Olympus objective, resulting in an approximately  $1 \mu\text{m}$  spot size in backscattering geometry. Raman measurements were performed using a 632.8 nm He-Ne laser with an 1800 l/mm grating, while photoluminescence measurements were performed using a 532 nm Nd:YAG laser with a 150 l/mm grating. TEM investigations were performed using an imaging corrected FEI Titan 80-300 microscope operating at 300 kV. The samples were prepared by a classical procedure using mechanical polishing followed by ion milling.

### 3. Results and Discussion

Before discussing the growth of GaSe it is important to recognize the possible polytypes of GaSe since any one of them may be selected by the prepared substrate. GaSe is a layered group-III chalcogenide semiconductor that crystallizes in several polytypes, distinguished by the stacking sequence of Se-Ga-Ga-Se tetralayers along the crystallographic *c*-axis as shown in Fig. 1.

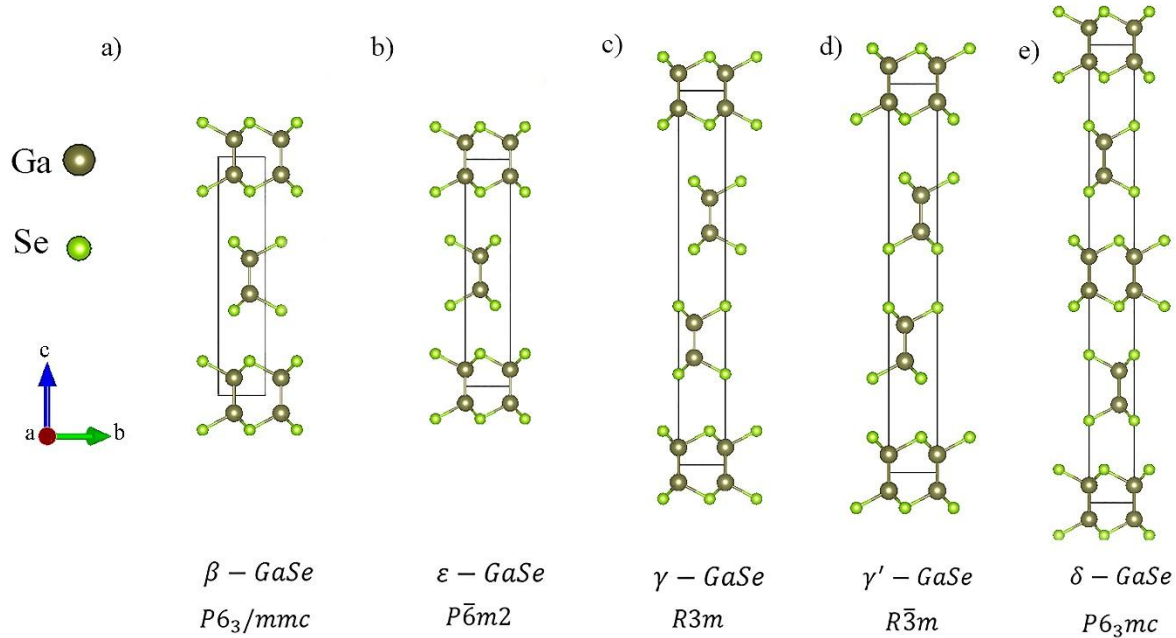


**Fig. 1.** Unit cells (black rectangles) of representative GaSe polytypes: (a)  $\beta - \text{GaSe}$ , (b)  $\varepsilon - \text{GaSe}$ , (c)  $\gamma - \text{GaSe}$ , (d)  $\gamma' - \text{GaSe}$ , (e)  $\delta - \text{GaSe}$ . Gallium atoms are shown in brown and selenium atoms in green. Crystallographic axes are indicated for reference.

The most commonly observed polytypes are the  $\varepsilon$ -GaSe (hexagonal, space group  $P6_3/mmc$ ) and  $\gamma$ -GaSe (rhombohedral, space group  $R3m$ ) phases, while rarer variants such as  $\gamma'$ -GaSe and  $\beta$ -GaSe have also been reported<sup>18-20</sup>. Despite sharing nearly identical in-plane lattice parameters, these polytypes differ in their out-of-plane stacking and inversion symmetry. Differences in stacking energetics are only on order of a few meV per atom, which allows multiple polytypes to coexist at growth interfaces<sup>19, 21</sup>. With these possibilities in mind, we discuss using the four sets of

GaAs(211)B and GaAs(001)B prepared substrates to grow GaSe and examine the role and nature of the substrate surface on the GaSe growth morphology and GaSe/GaAs interface.

### 3.1. Growth of GaSe on GaAs(211) with different surface conditions

The GaAs(211) surface is a high-index crystallographic plane that can be described as a corrugated topology composed of alternating terraces and steps (Fig. 2a) with the (211) plane intersecting the (111) plane at an angle of  $19.46^\circ$ , that exposes both Ga and As atoms (see Supplementary Material, Fig. S1).

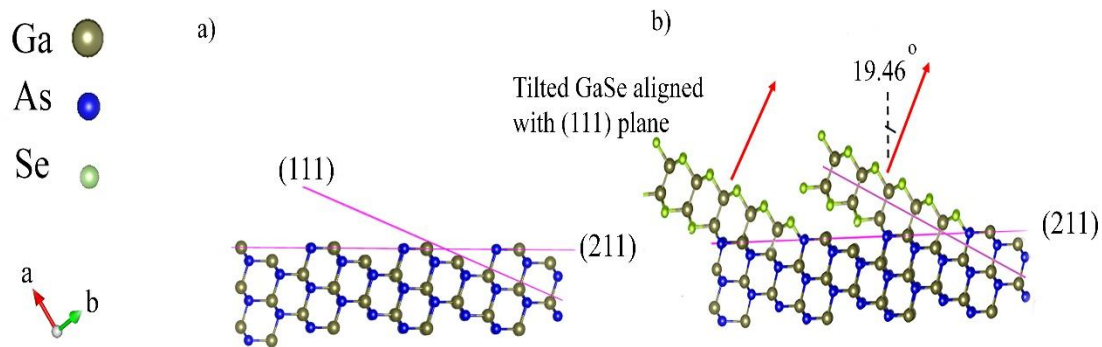


**Fig. 2.** Chemical structure of (a) oxide-free and defect-free GaAs(211) substrate; (b) GaSe grown on oxide-free and defect-free GaAs(211) substrate evidencing the angle of  $19.46^\circ$  degrees that GaSe film makes with GaAs(211) substrate. The brown sphere is Ga, the blue sphere is As, and the green sphere is Se. The bond lengths for Ga-As and Ga-Se are nearly the same. The red arrow indicates the direction normal to the (111) surface.

Below, we discuss the growth of GaSe on the four sets of prepared epi-ready GaAs(211) substrates:

**(a) Set 1 - oxide removed:** Due to the covalent nature of GaAs bonding, oxygen readily forms covalent bonds with either surface As or Ga atoms, depending on the surface termination. On the GaAs(211) surface, where both Ga and As atoms are exposed, both oxides can form although it is likely that only Ga remains after the oxide desorption<sup>22, 23</sup>. Before growth, RHEED

from GaAs oxidized surfaces exhibit ring-shaped patterns, characteristic of an amorphous or poorly ordered oxide surface<sup>24</sup>. After removing the oxide layer from the substrate by heating at 580-620 °C for 10 min, the RHEED pattern (Fig. 3a) exhibits a well-defined dotted pattern, characteristic of a rough 3D GaAs surface<sup>25</sup>, along with the step feature corresponding to a GaAs(211) surface.

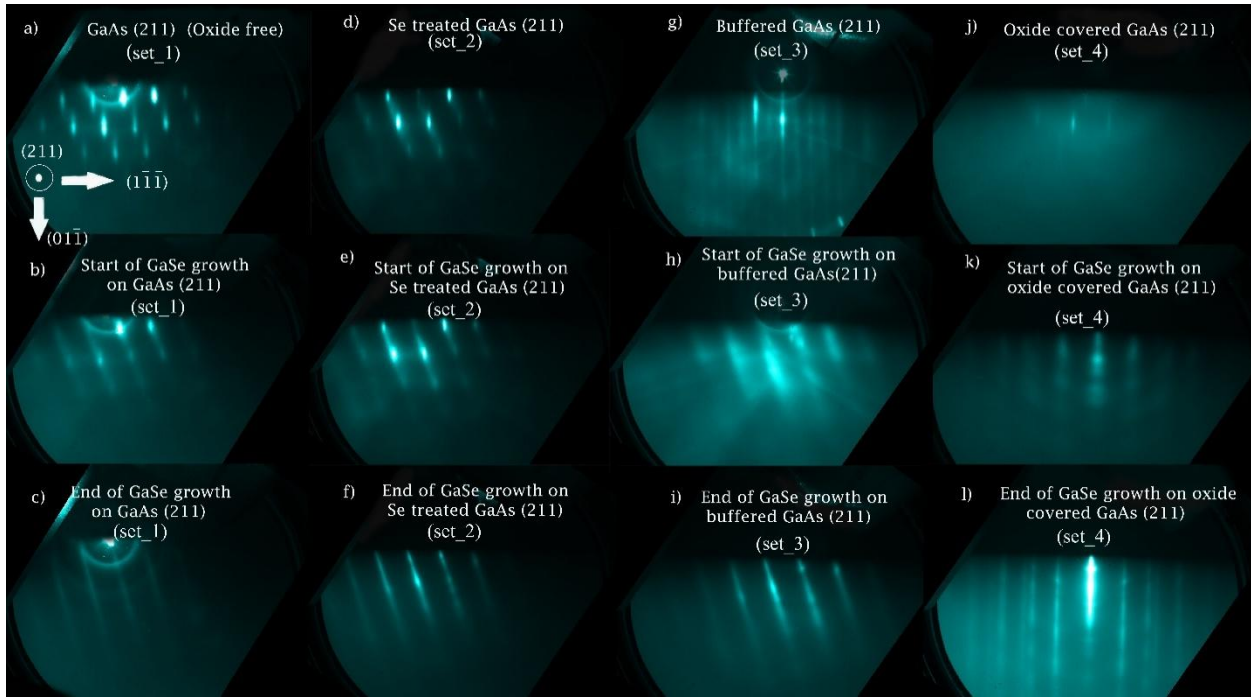


**Fig. 3.** RHEED pattern of GaAs(211) substrates and GaSe films under various surface preparation conditions: (a) oxide-free GaAs(211) substrate; (b) beginning of GaSe growth on oxide-free GaAs(211) substrate; (c) end of growth of GaSe on oxide-free GaAs(211) substrate; (d) Se treated oxide-free GaAs(211) substrate; (e) beginning of GaSe growth on Se treated oxide-free GaAs(211) substrate; (f) end of GaSe growth on Se treated oxide-free GaAs(211) substrate; (g) buffered GaAs(211) substrate; (h) beginning of GaSe growth on buffered GaAs(211) substrate; (i) end of growth of GaSe on buffered GaAs(211) substrate; (j) oxide covered GaAs(211) substrate, (k) beginning of GaSe growth on oxide covered GaAs(211) substrate; (l) end of growth of GaSe on oxide covered GaAs(211) substrate.

At the onset of GaSe growth, immediately after opening the Ga and Se shutters, distinct tilted lines appear in the RHEED pattern (see Fig. 3b) and persist throughout the deposition (see Fig. 3c). AFM images of the 2D GaSe grown on the oxide-free surface reveal long, tilted structures (see Fig. 4b). The RHEED acquired along  $[1\bar{1}\bar{1}]$  azimuthal in GaAs(211), shows a tilt angle of

about 20° (see Supplementary Material, Fig. S2). Likewise, the AFM line profile also shows a tilted GaSe 2D film growth with an approximate angle of ~20° from the substrate (211) plane, along GaAs (111) direction, (see Supplementary Material, Fig. S3). The tilt angle of GaSe 2D films relative to the substrate normal is similar to the angle between the GaAs(111) and GaAs(211) planes, which we calculate to be 19.46° (see Fig. 1 and Supplementary Material, Fig. S1). The outcome, therefore, is suspected to be growth of separated 2D planes at an angle of about 20° to the substrate normal as depicted in Fig. 2b. To support this hypothesis, we examined XRD. The XRD 2θ- $\omega$  scans of GaSe grown on GaAs(211) without a native oxide layer and with the diffraction vector aligned normal to the (211) surface, revealed that there was no GaSe Bragg diffraction (Fig. 5a). However, when the sample was tilted in only one specific direction such that the diffraction vector becomes normal to the (111) plane of the (211) substrate, characteristic XRD peaks of GaSe emerged (Fig. 5b, orange curve). Additionally, we speculate that the short interruptions observed in the AFM image of the planes are correlated to nucleation affected by the roughness of the initial GaAs surface. Meanwhile, the Raman spectrum further confirms the crystal quality. For example, the Raman spectrum from the tilted 2D films (Fig. 5e, orange curve) indicated the characteristic modes of  $\varepsilon$ -GaSe polytype of  $A_{1g}^1 \sim 133.2 \text{ cm}^{-1}$ ,  $E_{2g}^2 \sim 207.0 \text{ cm}^{-1}$ ,  $A_2'' \sim 247.0 \text{ cm}^{-1}$ ,  $E_{2g}^1 \sim 252.0 \text{ cm}^{-1}$  and  $A_{1g}^2 \sim 307.0 \text{ cm}^{-1}$ , approximately<sup>15, 26-29</sup>. GaAs modes of TA~160.0  $\text{cm}^{-1}$ , TO~268.0  $\text{cm}^{-1}$ , and LO~292.0  $\text{cm}^{-1}$  are also observed<sup>30, 31</sup>.

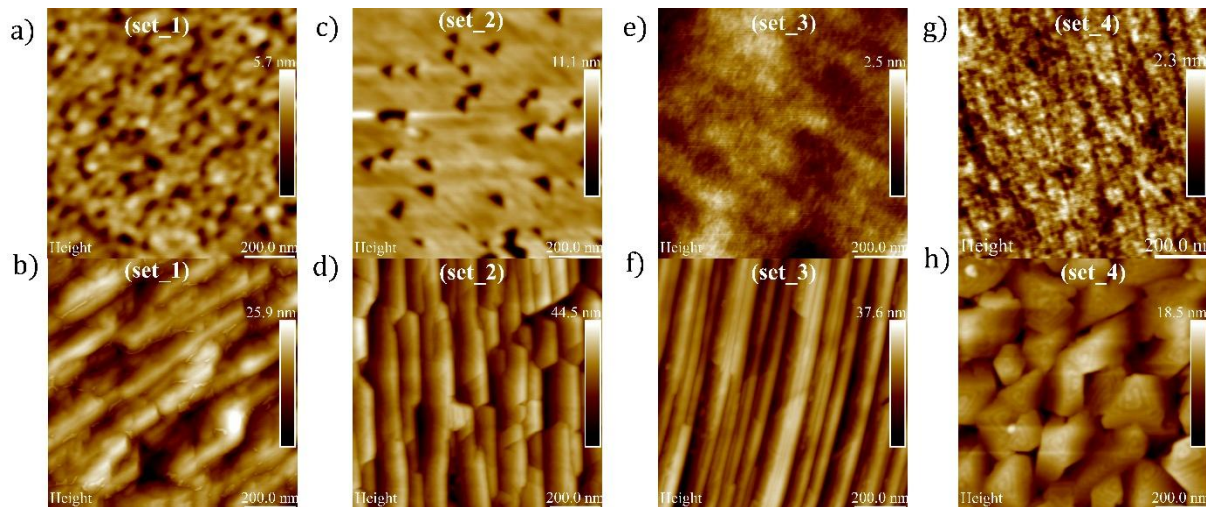


**Fig. 4.** Atomic Force Microscopy of surfaces of GaAs(211) substrates and GaSe films under various surface preparation conditions: (a) oxide-free GaAs(211); (b) GaSe film on oxide-free GaAs(211); (c) Se treated oxide-free GaAs(211); (d) GaSe film growth on oxide-free Se treated GaAs(211); (e) buffered GaAs(211); (f) GaSe film growth on buffered GaAs (211); (g) oxide covered GaAs(211) substrate; (h) GaSe film growth on oxide covered GaAs(211).

**(b) Set 2 - Oxide removed under Se Flux:** Removing the GaAs(211) surface oxide layer in the presence of an excess Se flux enables Se atoms to potentially occupy the resulting surface As vacancies (as indicated by XPS, see Supplementary Material, Fig. S4) forming GaSe at the surface of the substrate<sup>32</sup>. Both RHEED and AFM indicate the growth of tilted 2D GaSe planes. However, they appear to be more coherently ordered, marking a clear progression in crystalline quality relative to the previous set (see Fig. 5b, green curve). The key difference from the oxide removal set is that the smoother starting surface (ignoring the triangular distortion) results in nucleation of GaSe layers that are more ordered and aligned, and thus more neatly stacked (see Fig. 4d). Our hypothesis is that when GaSe forms at the GaAs substrate surface<sup>32, 33</sup>, Se replaces As or As vacancies at the interface producing a smoother epitaxial starting surface that supports the formation of more ordered 2D GaSe planes, (Supplementary Material, Figs. S4 and S5). This hypothesis was examined with XPS (Supplementary Material, Figs. S4 and S5), which indicated that for a GaAs substrate that is exposed to Se before growth of GaSe, there is a decrease in As

with a corresponding increase in Se, in agreement with our hypothesis. The Raman spectrum for Set 2 exhibits the same characteristic  $\epsilon$ -GaSe phonon modes observed in Set 1 of  $A_{1g}^1 \sim 133.2 \text{ cm}^{-1}$ ,  $E_{2g}^2 \sim 207.0 \text{ cm}^{-1}$ ,  $A''_2 \sim 247.0 \text{ cm}^{-1}$ ,  $E_{2g}^1 \sim 252.0 \text{ cm}^{-1}$ ,  $A_{1g}^2 \sim 307.0 \text{ cm}^{-1}$ . The primary distinction is that the  $E_{2g}^1 \sim 252.0 \text{ cm}^{-1}$  shows a noticeably stronger peak relative to the other modes and compared with all other sample sets (see Fig. 5e, green curve).

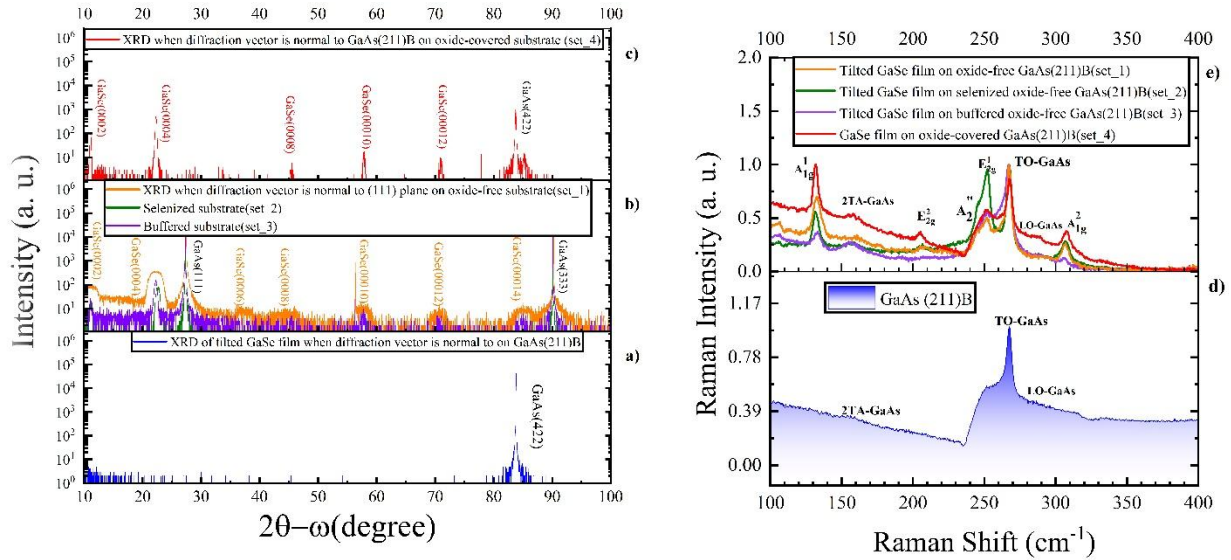


**Fig. 5.** Structural and vibrational characterization of GaSe films grown on GaAs(211)B under different surface preparation conditions. (a) XRD pattern of tilted GaSe grown on GaAs(211)B, measured with the diffraction vector normal to the GaAs(211) plane. (b) XRD pattern of tilted GaSe films grown on oxide-free (set-1), selenized oxide-free (set-2), and buffered oxide-free (set-3) GaAs(211)B, measured with the diffraction vector normal to the GaAs(111) plane. (c) XRD pattern of GaSe grown on an oxide-covered GaAs(211)B substrate (set-4), measured with the diffraction vector normal to the GaAs(211) plane. (d) Raman spectrum of the GaAs(211)B substrate. (e) Raman spectra of GaSe films grown on oxide-free (orange curve), selenized oxide-free (green curve), buffered oxide-free (purple curve), and oxide-covered (red curve) GaAs(211)B substrates.

Likewise, direct imaging of the atomic order via TEM in Fig. 6 also confirms the crystal quality and tilted growth of the GaSe film at angle of about  $20^\circ$  from the substrate interface. Interestingly, certain regions exhibit a uniform  $\epsilon$ -GaSe structure although defects are present (see the red rectangle in the inset of Fig. 6a. Basically, we observe an outcome similar to set-1 except for the

more ordered array of 2D GaSe plane, consistent with our hypothesis of the impact of surface smoothness on coherent 2D growth.

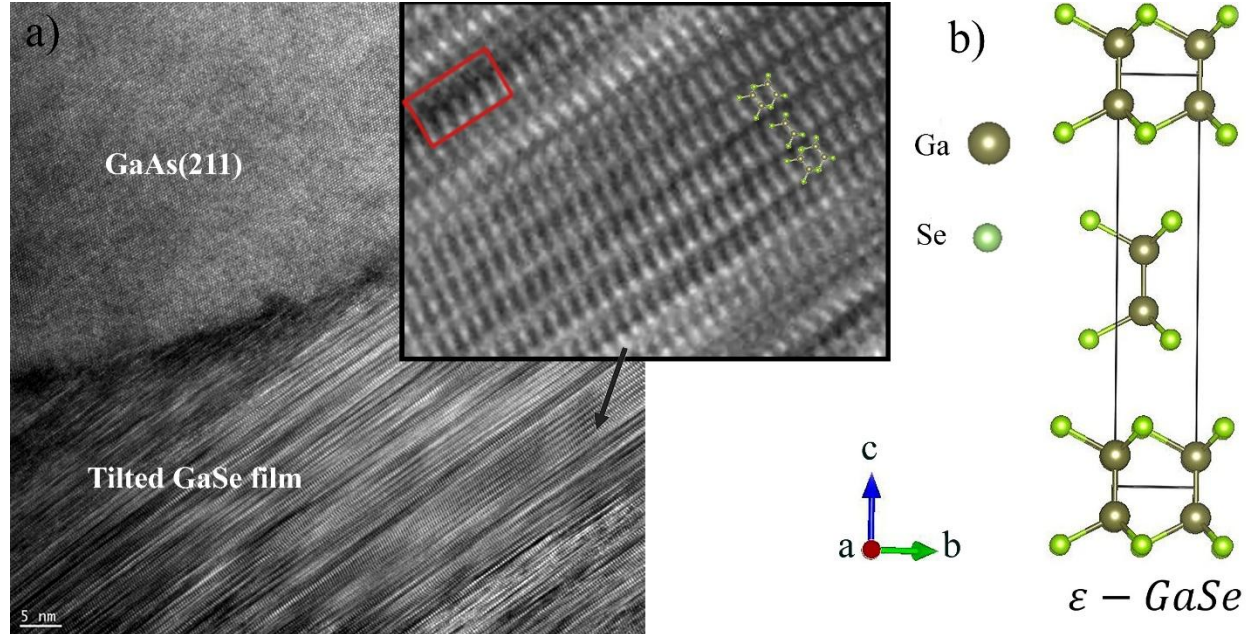


**Fig. 6.** (a) Cross-sectional TEM image showing tilted two-dimensional GaSe growth on oxide-free GaAs(211). The inset shows a magnified region where the atomic stacking sequence corresponding to the  $\varepsilon$ -GaSe polytype is observed. The black rectangle highlights the region used for polytype identification, while the red rectangle indicates the presence of a stacking fault. (b) Crystal structure and unit cell of  $\varepsilon$ -GaSe for reference.

**(c) Set 3 - Oxide removed and GaAs buffer added:** Depositing a GaAs buffer layer prior to GaSe growth also potentially modifies the interface. In this case, both Ga and As atoms are present at the surface since the buffer layer is deposited at about 580°C and then lowered to the GaSe growth temperature while under As flux. The RHEED pattern of the buffer layer (see Fig. 3g) exhibits much longer, well-defined streaks, indicating an atomically smooth surface<sup>25</sup>. Upon initiating GaSe growth by simultaneously opening the Ga and Se effusion cell shutters, the RHEED pattern immediately transitions to a tilted configuration (see Fig. 3h), suggesting a change in growth orientation. The angle observed in the RHEED pattern is again about  $\sim 20^\circ$  and the GaSe

layers also grow tilted in this case. Introducing a buffer layer however, produces an atomically smooth surface for GaSe growth planes resulting in even more uniform 2D planes (Fig. 4f). Comparing the AFM images in Figs. 4b, 4d, 4f clarifies the evolution of morphology. Oxide removal yields tilted ridges, adding Se during oxide removal elongates these ridges and enhances faceting, and with a buffered surface, the ridges become highly uniform and crystalized which is confirmed with XRD (Fig. 5b, purple curve). Across all three substrate conditions, (a) oxide-free, (b) Se, and (c) buffered surfaces, the 2D GaSe films are tilted relative to the substrate within a growth temperature window of 350-500°C. Once the native oxide is removed the film consistently adopts the tilted orientation consistent with a lattice match and bonding at the surface.

**(d) Set 4 - Native oxide layer not removed:** For the oxide prepared GaAs surface the observed RHEED pattern is a ring-shaped pattern (Fig. 3j), signaling an amorphous or poorly ordered surface. Upon initiating GaSe growth on this surface, the RHEED pattern shows faint, broadened features (Fig. 3h), indicative of misoriented nucleation and surface disorder<sup>34</sup>. This is of course a significant difference compared to sets 1-3. At the end of growth, the RHEED pattern becomes straight and streaky, indicating that the film growth is potentially along the c-axis<sup>25</sup>, in contrast to the oxide-free surface where tilted streaks are observed. XRD 2θ-ω scans with the diffraction vector normal to the (211) surface reveals GaSe Bragg reflections, confirming that the film adopts a (0001) orientation on the oxide-covered GaAs(211) substrate, see Fig. 5c. Likewise, we also investigate the Raman spectrum to further examine the growth direction and crystal quality. As shown in Fig. 5e (red curve), the film with its c-axis perpendicular to the substrate exhibits the same characteristic GaSe Raman modes observed in the tilted film of  $A_{1g}^1 \sim 133.2 \text{ cm}^{-1}$ ,  $E_{2g}^2 \sim 207.0 \text{ cm}^{-1}$ ,  $A_2'' \sim 247.0 \text{ cm}^{-1}$ ,  $E_{2g}^1 \sim 252.0 \text{ cm}^{-1}$ , and

$A_{1g}^2 \sim 307.0 \text{ cm}^{-1}$ <sup>15, 26, 30, 31</sup>. In addition, we investigated AFM and TEM to probe crystal quality and tilted growth. The AFM topography (Fig. 4h) reveals triangular, layer-like morphologies consistent with 2D spiral growth<sup>35</sup> attributed to the roughness of the surface which promotes heterogeneous nucleation<sup>22</sup> and step-spiral propagation. TEM images (see Fig. 7) also reveal directly that the set 4 of 2D GaSe films are tilt-free. It also indicates that as the distance for growth from the interface increases, the crystal structure becomes more uniform, potentially indicating a gradual transition toward a single dominant polytype (see Fig. 7b). Specifically, the  $\gamma'$ -GaSe polytype<sup>19</sup> is observed using set 4 prepared substrates, see Fig. 7b-c.

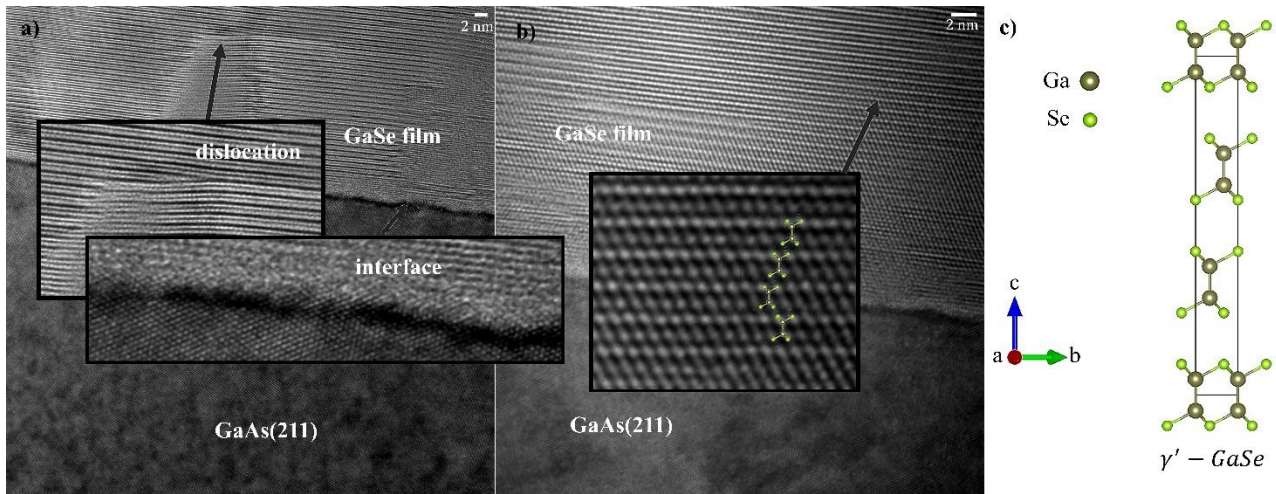


**Fig. 7.** Cross-sectional TEM images of GaSe grown on oxide-covered GaAs(211). (a) TEM image showing a dislocation originating at the oxide-covered interface. The highlighted rectangular region indicates interfacial nonuniformity, where bonding is not spatially uniform; (b) High-resolution TEM image revealing the  $\gamma'$  - GaSe polytype, with the inset highlighting the atomic stacking sequence; (c) Crystal structure schematic of the  $\gamma'$  - GaSe polytype for reference,

PL measurements were also taken to evaluate the optical quality of the GaSe films grown on GaAs(211)B under various surface preparation conditions. As shown in Fig. 8, all spectra are dominated by the GaAs bandgap emission near 800 nm and a weak GaSe-related feature appears in the 670-750 nm range. This GaSe-related emission is at first absent for the sample sets with tilted planes due to the inefficient optical coupling to the GaSe layers and reduced extraction of

the emitted photoluminescence along the excitation direction<sup>36</sup>. As a result, the emission from tilted GaSe in Fig. 8 is detectable only when the sample is physically tilted by approximately 20° for excitation and collection normal to the planes.

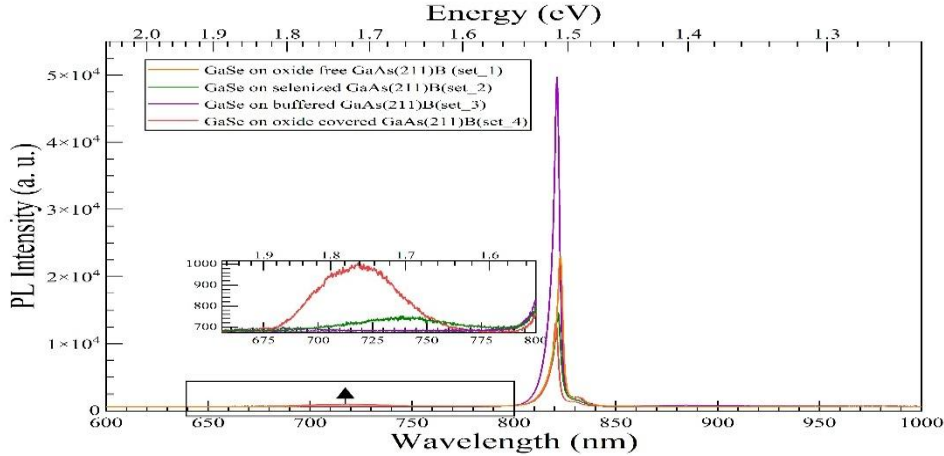


**Fig. 8.** PL intensity of GaSe on oxide-free GaAs(211) (orange curve), on selenized oxide-free GaAs(211) (green curve), on oxide-free buffered GaAs(211) (purple curve), and on oxide covered GaAs(211) (red curve).

In summary, our investigation of GaSe film growth by MBE on four differently prepared GaAs surfaces indicates that it is possible to grow 2D GaSe on a 3D GaAs(211) surface. However, (1) on oxide removed surfaces, due to systematic bonding, the morphology can be characterized by the growth of angled 2D GaSe planes that become more uniform over atomically smooth regions. And (2) on oxide covered surfaces since systematic bonding in general does not occur then the morphology can be characterized as c-axis 2D spiral-like plates spatially influenced by the variation in the substrate surface height. We speculate that if variations in the height of the substrate surface are not matched to the 2D c-axis lattice constant, nucleation at the interface can produce growth at different locations that are out of phase with one another leading to 2D spiral-like plates.

### 3.2. Growth of GaSe on GaAs(001) with different surface conditions

Based on the results for GaSe on GaAs(211), we also examined the growth of GaSe films on GaAs(001) which has also been investigated by several researchers with contrasting results. The GaAs(001) surface is a zincblende cut perpendicular to [001]. Its tetrahedral bonds point toward the  $\langle 111 \rangle$  family (Fig. 9a), so the outermost atoms include  $\langle 111 \rangle$  oriented dangling bonds that define chemically active sites for nucleation (Fig. 9b-d).

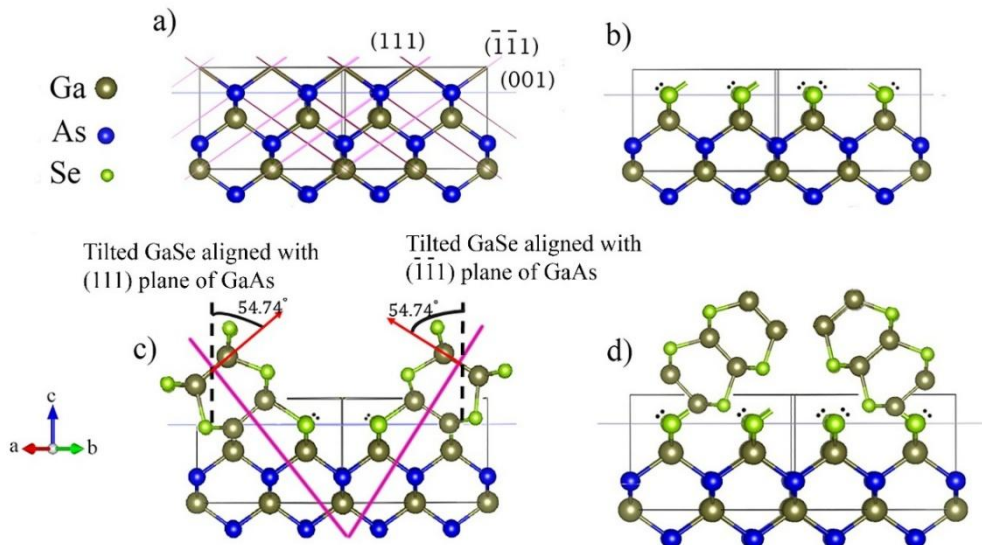


**Fig. 9.** (a) Dangling bonds on the GaAs(001) As-terminated prepared surface; (b) Se prepared surface with Se atoms replacing As atoms on the surface resulting in a Se-terminated GaAs(001) surface; (c) Possible tilted growth of GaSe on the As-terminated surface GaAs(001) in (a); (d) Possible tilted growth of GaSe on Se treated or Se-terminated GaAs(001) surface in (b).

Below, we discuss the growth of GaSe on four sets of prepared epi-ready GaAs(001) substrates:

**Set 1 - Oxide removed:** The GaAs(001) substrate is As-terminated before oxidation at As sites and the formation of insulating As oxides<sup>23</sup>. After thermal oxide removal at  $\sim 580^\circ\text{C}$ , the

substrate was cooled to the growth temperature of 400°C and is Ga-terminated. At the onset of deposition of GaSe, Se fills what were the As sites and tilted RHEED streaks appeared (Fig. 10b) that intensified during growth.

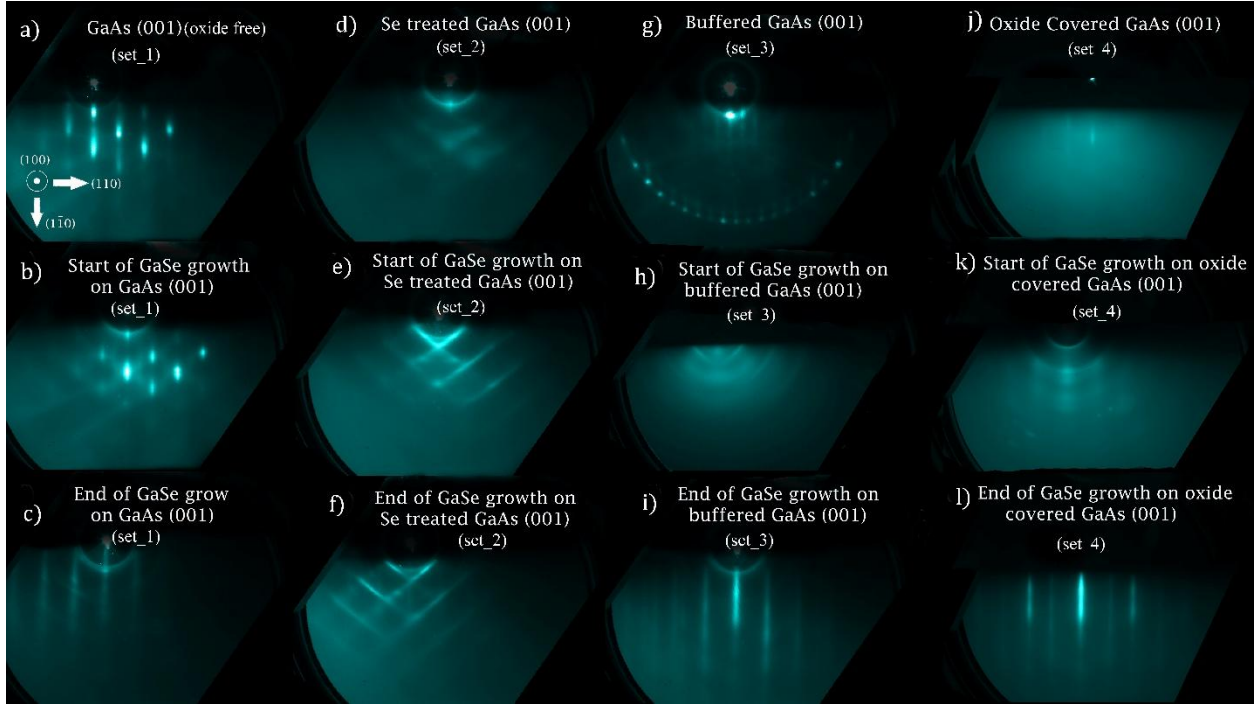


**Fig. 10.** RHEED patterns of GaAs(001) substrates and GaSe films under various surface preparation conditions: (a) Oxide-free GaAs(001) substrate; (b) Beginning of GaSe growth on oxide-free GaAs(001) substrate; (c) End of growth of GaSe on oxide-free GaAs(001) substrate; (d) Se treated oxide-free GaAs(001); (e) Beginning of GaSe growth on Se treated oxide-free GaAs(001) substrate; (f) End of GaSe growth on Se treated oxide-free GaAs(001) substrate; (g) Buffered GaAs(001) substrate; (h) Beginning of GaSe growth on buffered GaAs(001) substrate; (i) End of growth of GaSe on buffered GaAs(001) substrate; (j) Oxide covered GaAs(001) substrate; (k) Beginning of GaSe growth on oxide covered GaAs(001) substrate; (l) End of growth of GaSe on oxide covered GaAs(001) substrate.

This understanding is supported by XRD data that reveals that GaSe reflections are observed only when the sample is tilted by  $\sim 54.0^\circ$  (Fig. 12a) in either direction in the (010) plane, indicating that the GaSe (001) axis is inclined relative to the surface normal of the (001)-oriented GaAs substrate. In this case, the 2D GaSe (001) planes are aligned with two of the substrate's  $\langle 111 \rangle$  directions. On the GaAs(001) surface, each surface Ga atom presents two dangling bonds oriented towards two of the four  $\langle 111 \rangle$  directions. This geometric arrangement naturally selects

two of the four symmetry-equivalent variants, so GaSe nucleates on the surface in two tilted orientations (Fig. 9b, d) which of course can cause competition in growth. In fact, we first noted that line scans of AFM topographic images in Fig. 11b indicated the existence of tilted growth at about at  $\sim 54^\circ$  to the normal. This made us investigate samples with much lower depositions than shown in Fig. 11a, for which we more clearly observe tilted growth at  $\sim 54^\circ$  in both directions from the normal (insert of Fig. 11b). However, at the larger deposition shown in Fig. 11b, the competition between growth in both directions apparently leads to a merger into growth normal to the surface.

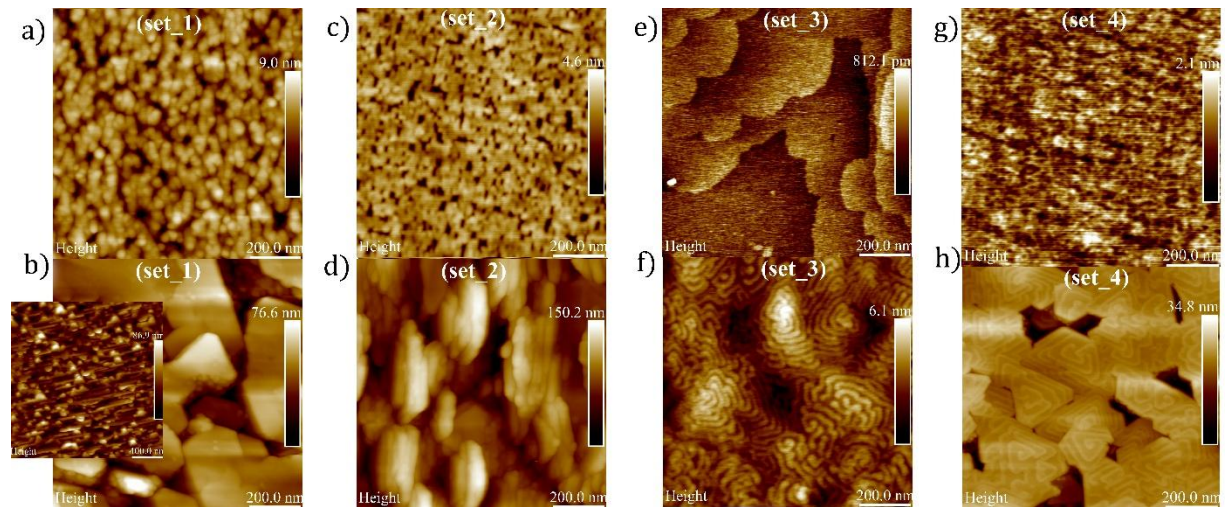


**Fig. 11.** Atomic microscopy of patterns of GaAs(001) substrates and GaSe films under various surface preparation conditions: (a) Oxide-free GaAs(001) substrate; (b) GaSe film on oxide-free GaAs(001) substrate; (c) Oxide-free GaAs(001) substrate with Se overflow; (d) GaSe film growth on oxide-free GaAs(001) substrate with Se overflow; (e) Buffered GaAs(001) substrate; (f) GaSe film growth on buffered GaAs(001) substrate; (g) Oxide covered GaAs(001) substrate; (h) GaSe film growth on oxide covered GaAs(001) substrate.

This understanding is further supported by the XRD analysis of Fig. 12a(1) which gives a diffraction signal normal to the surface and at  $\pm 54^\circ$  while Fig. 12a(2) is observed only at  $\pm 54^\circ$ . This understanding is also consistent with the RHEED image change from Fig. 10b to Fig. 10c. The result indicates that depending on growth thickness one can observe either tilted growth or growth perpendicular to the surface.

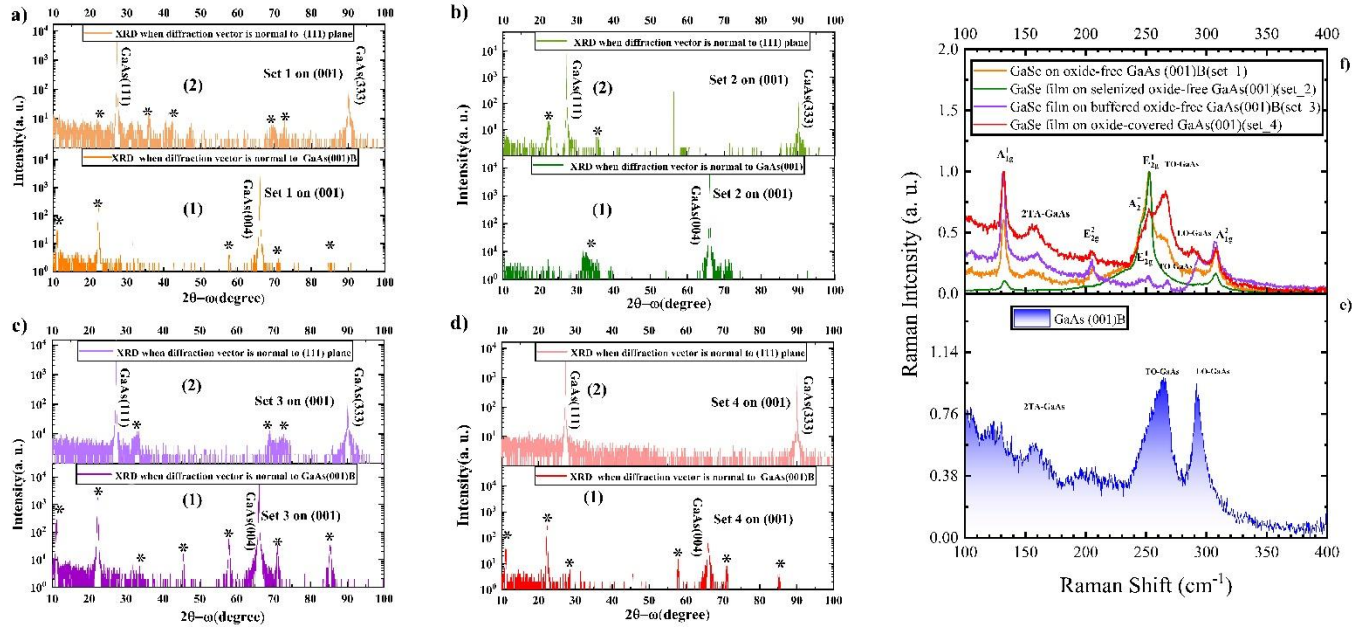


**Fig. 12.** XRD patterns of GaSe/GaAs(001) films with varying surface preparations. (a) Oxide-free; (b) selenized; (c) buffered; (d) oxide-covered. For each condition, scans were collected along (001) plane of GaAs(001), labeled as (1), and GaAs(111), labeled as (2). Asterisks indicate GaSe peaks. (e) Raman spectrum of the GaAs(001)B substrate. (f) Raman spectra of GaSe films grown on oxide-free (set-1, orange curve), selenized oxide-free (set-2, green curve), buffered (set-3, purple curve), and oxide-covered (set-4, red curve), as well as GaAs(001)B substrate (blue curve).

**Set 2 - Oxide removed under Se flux:** We examined GaSe films grown on GaAs(001) with surface selenization. The RHEED patterns recorded before, during, and after growth show intense tilted streaks for the selenized surface (Figs. 10d–f) (Supplementary Material, Figs. S5 and S6). AFM also reveals that alignment along two specific (111) directions of the GaAs(001) substrate (Fig. 11d) but not along (010) as in Fig. 11b. We attribute this to differences in surface termination. A Ga-terminated GaAs(001) surface presents two dangling bonds per atom, enabling both Ga and Se to bond, with Ga-Se bonding energetically favored (due to electronegativity difference), thereby allowing multiple tilted variants at different locations. In contrast, a Se adlayer provides only one dangling bond per Se atom, restricting nucleation to Ga-Se bonds and reducing the number of accessible variants and competition (due to Se bonding in GaSe which only bonds with Ga).

Consequently, the Se-terminated surface favors a selective tilted growth mode consistent with the RHEED observations and XRD (Figs. 10c, 10f, 12b(1), 12b(2) and Supplementary Material Figs. S5 and S6).

***Set 3 - Oxide removed and GaAs buffer added:*** We now consider the case of growing an As-terminated GaAs buffer layer on an oxide-free GaAs(001) substrate. The oxide is again removed at about 580°C in the presence of As creating an As-terminated (001) surface. The sample was then lowered to the GaSe growth temperature in As. The growth begins with tilted GaSe layers at  $\sim 54^\circ$  but followed by a transition into c-axis-oriented GaSe aligned perpendicular to the (010) plane (See Fig. 10h). This observation is further confirmed by XRD measurements, as shown in Fig. 12c(1) and Fig. 12c(2), where GaSe Bragg diffraction peaks are present when the diffraction vector is perpendicular to the (001) and all four (111) planes. The resulting morphology under these growth conditions is characterized by 2D spiral growth, as shown in Fig. 11f, apparently due to angled growth merging from four directions. The films quality of oxide free samples are again confirmed by the characteristic Raman active modes of GaSe ( $A_{1g}^1 \sim 133.2 \text{ cm}^{-1}$ ,  $E_{2g}^2 \sim 207.0 \text{ cm}^{-1}$ ,  $A_2'' \sim 246.0 \text{ cm}^{-1}$ ,  $E_{2g}^1 \sim 252.0 \text{ cm}^{-1}$ ,  $A_{1g}^2 \sim 307.0 \text{ cm}^{-1}$ ), as expected.

***Set 4 – Native oxide layer not removed:*** For GaSe films grown by MBE on a (001)-oriented GaAs substrate with its native oxide layer, our observation is similar to those for growth on a GaAs(211) substrate with its native oxide layer. The initial RHEED pattern is ring-shaped (Fig. 10j), which evolves into straight streaks by the end of growth (Fig. 10l). This, alongside with the XRD pattern in Fig. 12d, confirms that GaSe films adopt a (001) orientation without tilt growth. Raman spectroscopy in Fig. 12f shows that the characteristic modes of GaSe have low intensity compared to GaAs modes. Meanwhile, AFM topography images, in Fig. 11h, reveal the triangular

helicoidal features that were also observed previously. As shown in Fig 13 we also investigated the PL from the four sample sets. Similarly to the PL seen in Fig. 8, the observed emissions covered different spectral regions for substrates that were prepared under different surface conditions. Tilted growth samples tended to have a higher energy component to the spectrum which we speculate can be due to the thickness of the 2D layer<sup>37</sup>.

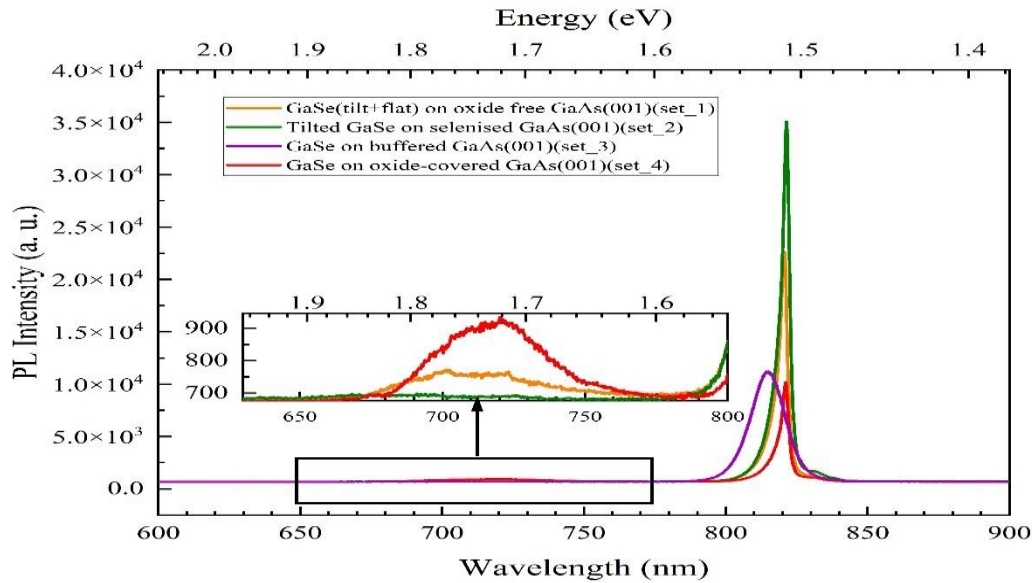


**Fig. 13.** PL intensity of GaSe on oxide-free GaAs (001, on selenized GaAs(001), and on oxide covered GaAs(001).

In summary, the growth of GaSe on GaAs(001) is more complicated than growth on GaAs(211) due to competition for nucleation in two and four different directions. However, the outcome has some similar points to make: (1) if systematic bonding occurs the morphology will be characterized by the growth of angled 2D GaSe planes that can be more uniform over atomically smooth regions. However, there can be competition between growth at different angles resulting in a compromised growth along the c-direction and in set 3 growth characterized by 2D spiral plates. And (2) if systematic bonding does not occur then the morphology will be characterized by 2D spiral-like plates. In all cases, the morphology of growth is highly dependent on the atomic

smoothness and step nature of the surface, as might be expected for 2D layer growth. This can explain the differences in previous reports for growth on GaAs(001). Although no details are given here, we also probed growth on the high index GaAs surfaces of GaAs(311) and (411) and found similar and consistent results briefly summarized in Table I and Table S.I in Supplementary Material.

**Table I. GaSe Growth mode on GaAs(211) and (001) with different interfacial condition**

<i>Substrates</i>	<i>Oxide removed</i>	<i>Se treated</i>	<i>Buffered</i>	<i>Oxide covered</i>
GaAs(211)	Growth angle (19.46°)	Growth angle (19.46°)	Growth angle (19.46°)	2D spiral growth
GaAs(001)	Growth angle (54.73°)	Growth angle (54.73°)	2D spiral growth	2D spiral growth

#### 4. Conclusion

In this work, we establish that interfacial bonding chemistry, rather than growth kinetics alone, fundamentally governs the epitaxy of GaSe on 3D GaAs substrates. By systematically comparing GaAs(211)B and GaAs(001)B substrates under controlled surface chemistries, including native oxide, oxide removal, Se pre-exposure, and GaAs buffer layers, we directly identify the interfacial mechanisms that select growth mode, crystallographic orientation, and polytype evolution in 2D/3D heterostructures. We have identified a deterministic orientation-selection mechanism linking substrate symmetry and dangling-bond coordination to layered GaSe growth. We show that oxide-free GaAs(211) promotes tilted quasi-layered GaSe growth with a characteristic tilt of  $\sim 19.46^\circ$ , while Se termination and buffer layers enhance epitaxial coherence without altering the tilt selection. In contrast, native oxide surfaces suppress systematic interfacial bonding, leading to non-tilted spiral growth and interfacial polytype mixing. On GaAs(001),

surface termination determines whether growth proceeds through symmetry-allowed tilted variants ( $\sim 54.7^\circ$ ) or transitions to non-tilted spiral growth through heterogeneous nucleation pathways. These results resolve the long-standing ambiguity between tilted and non-tilted 2D growth on 3D semiconductor platforms. More broadly, this work provides the first unified mechanistic framework describing how interfacial bonding and surface symmetry control layered 2D/3D heteroepitaxy. The demonstration that substrate orientation defines allowable epitaxial variants while surface termination selects growth mode establishes a generalizable interface-engineering strategy. This framework enables deterministic control of orientation, defect density, and polytype selection, providing a pathway toward wafer-scale integration of layered chalcogenides with established semiconductor manufacturing platforms for optoelectronic, nonlinear optical, and quantum device applications.

## ACKNOWLEDGEMENTS

The authors acknowledge partial support from  $\mu$ -ATOMS, an Energy Frontier Research Center funded by the U.S. Department of Energy (DOE), Office of Science, Basic Energy Sciences (BES), under award DE-SC0023412, a grant from the Air Force Office of Scientific Research through award no. FA9550-24-1-0263, and the National Science Foundation under Grant No. DGE-2244274. We also acknowledge the MonArk NSF Quantum Foundry supported by the National Science Foundation Q-AMASE-i program under NSF award No. DMR-1906383.

## CONFLICT OF INTEREST

The authors declare that they have no conflict of interest.

## REFERENCES

- (1) Wu, Y.; Fuh, H.-R.; Zhang, D.; Coileáin, C. Ó.; Xu, H.; Cho, J.; Choi, M.; Chun, B. S.; Jiang, X.; Abid, M.; et al. Simultaneous large continuous band gap tunability and photoluminescence enhancement in GaSe nanosheets via elastic strain engineering. *Nano Energy* **2017**, *32*, 157-164. DOI: <https://doi.org/10.1016/j.nanoen.2016.12.034>.
- (2) Barker, T.; Gray, A.; Weir, M. P.; Sharp, J. S.; Kenton, A.; Kudrynskyi, Z. R.; Rostami, H.; Patané, A. Giant elasto-optic response of gallium selenide on flexible mica. *npj Flexible Electronics* **2025**, *9* (1). DOI: <https://doi.org/10.1038/s41528-024-00375-3> (accessed 2026-02-11T15:19:46).
- (3) Fadlallah, M. M.; Abdel-Azeim, S. Study on substitutional doped GaSe monolayers using hybrid functional: Electronic, optoelectronic, and photocatalytic applications. *Materials Science in Semiconductor Processing* **2026**, *201*, 110068. DOI: <https://doi.org/10.1016/j.mssp.2025.110068>.
- (4) Singh, N. B.; Kanner, G.; Marable, M.; Berghmans, A.; Knuteson, D.; Kahler, D.; Wagner, B.; King, M. Selenides for nonlinear optical applications. *Emerging Materials Research* **2012**, *1* (4), 185-200. DOI: <https://doi.org/10.1680/emr.11.00012> (accessed 2025/06/23).
- (5) Zhou, X.; Cheng, J.; Zhou, Y.; Cao, T.; Hong, H.; Liao, Z.; Wu, S.; Peng, H.; Liu, K.; Yu, D. Strong Second-Harmonic Generation in Atomic Layered GaSe. *Journal of the American Chemical Society* **2015**, *137* (25), 7994-7997. DOI: <https://doi.org/10.1021/jacs.5b04305>.
- (6) Lin, Y.-C.; Torsi, R.; Younas, R.; Hinkle, C. L.; Rigos, A. F.; Hill, H. M.; Zhang, K.; Huang, S.; Shuck, C. E.; Chen, C.; et al. Recent Advances in 2D Material Theory, Synthesis, Properties, and Applications. *ACS Nano* **2023**, *17* (11), 9694-9747. DOI: <https://doi.org/10.1021/acsnano.2c12759>.
- (7) Qi, X.; Gao, M.; Ding, C.; Zhang, W.; Qu, R.; Guo, Y.; Gao, H.; Zhang, Z. Simple Exfoliation of Bulk Gallium Selenide to Single/Few Layers by a Temperature-Adjustment Bath-Ultrasonic Treatment. *physica status solidi (RRL) – Rapid Research Letters* **2021/08/01**, *15* (8). DOI: <https://doi.org/10.1002/pssr.202100052>.
- (8) Kowalski, B. M.; Manz, N.; Bethke, D.; Shaner, E. A.; Serov, A.; Kalugin, N. G. Role of humidity in oxidation of ultrathin GaSe. **2019**. DOI: <https://doi.org/10.1088/2053-1591/ab1dd2>.
- (9) Bergeron, A.; Ibrahim, J.; Leonelli, R.; Francoeur, S. Oxidation dynamics of ultrathin GaSe probed through Raman spectroscopy. *Applied physics letters* **2017**, *110* (24).
- (10) Jie, W.; Hao, J. Two-Dimensional Layered Gallium Selenide: Preparation, Properties, and Applications. In *Advanced 2D Materials*, 2016; pp 1-36.
- (11) Rumaner, L. E.; Gray, J. L.; Ohuchi, F. S. Nucleation and growth of GaSe on GaAs by Van der Waal epitaxy. *Journal of Crystal Growth* **1997**, *177* (1), 17-27. DOI: [https://doi.org/10.1016/S0022-0248\(96\)00970-0](https://doi.org/10.1016/S0022-0248(96)00970-0).
- (12) Abe, H.; Ueno, K.; Koichiro Saiki, K. S.; Atsushi Koma, A. K. Heteroepitaxial Growth of Layered GaSe Films on GaAs(001) Surfaces. *Japanese Journal of Applied Physics* **1993**, *32* (10A), L1444. DOI: <https://doi.org/10.1143/JJAP.32.L1444>.
- (13) Kojima, N.; Sato, K.; Yamada, A.; Konagai, M.; Kiyoshi Takahashi, K. T. Epitaxial Growth of GaSe Films by Molecular Beam Epitaxy on GaAs(111), (001) and (112) Substrates. *Japanese Journal of Applied Physics* **1994**, *33* (10B), L1482. DOI: <https://doi.org/10.1143/JJAP.33.L1482>.
- (14) Sorokin, S. V.; Avdienko, P. S.; Sedova, I. V.; Kirilenko, D. A.; Yagovkina, M. A.; Smirnov, A. N.; Davydov, V. Y.; Ivanov, S. V. Molecular-Beam Epitaxy of Two-Dimensional GaSe Layers

on GaAs(001) and GaAs(112) Substrates: Structural and Optical Properties. *Semiconductors* **2019**, *53* (8), 1131-1137. DOI: <https://doi.org/10.1134/S1063782619080189>.

(15) Diep, N. Q.; Liu, C.-W.; Wu, S.-K.; Chou, W.-C.; Huynh, S. H.; Chang, E. Y. Screw-Dislocation-Driven Growth Mode in Two Dimensional GaSe on GaAs(001) Substrates Grown by Molecular Beam Epitaxy. *Scientific Reports* **2019**, *9* (1), 17781. DOI: <https://doi.org/10.1038/s41598-019-54406-5>.

(16) Künzel, H. Molecular beam epitaxy of III-V compounds. *Physica B+C* **1985**, *129* (1), 66-80. DOI: [https://doi.org/10.1016/0378-4363\(85\)90555-8](https://doi.org/10.1016/0378-4363(85)90555-8).

(17) Wangila, E.; Gunder, C.; Zamani-Alavijeh, M.; Maia De Oliveira, F.; Kryvyi, S.; Sheibani, A.; Mazur, Y. I.; Yu, S.-Q.; Salamo, G. J. High-Quality Single-Step Growth of GaAs on C-Plane Sapphire by Molecular Beam. *Crystals* **2024**, *14* (8), 724. DOI: <https://doi.org/10.3390/cryst14080724>.

(18) Lee, C. H.; Krishnamoorthy, S.; O'Hara, D. J.; Brenner, M. R.; Johnson, J. M.; Jamison, J. S.; Myers, R. C.; Kawakami, R. K.; Hwang, J.; Rajan, S. Molecular beam epitaxy of 2D-layered gallium selenide on GaN substrates. *Journal of Applied Physics* **2017**, *121* (9), 094302. DOI: <https://doi.org/10.1063/1.4977697> (accessed 1/12/2024).

(19) Grzonka, J.; Claro, M. S.; Molina-Sánchez, A.; Sadewasser, S.; Ferreira, P. J. Novel Polymorph of GaSe. *Advanced Functional Materials* **2021**, *31* (48), 2104965. DOI: <https://doi.org/10.1002/adfm.202104965> (accessed 2024/02/18).

(20) Yu, M.; Iddawela, S. A.; Wang, J.; Hilse, M.; Thompson, J. L.; Hickey, D. R.; Sinnott, S. B.; Law, S. Quasi-Van der Waals Epitaxial Growth of  $\gamma'$ -GaSe Nanometer-Thick Films on GaAs(111)B Substrates. *ACS Nano* **June 13, 2024**, *18* (26). DOI: <https://doi.org/10.1021/acsnano.4c04194>.

(21) Materials Data on GaSe by Materials Project. United States, 2020.

(22) Ghita, R. V. Evolution of surface oxides on GaAs. *Journal of Optoelectronics and Advanced Materials* **2015**, *17* (11-12), 1703-1709.

(23) Lucovsky, G. A chemical bonding model for the native oxides of the III-V compound semiconductors. *Journal of Vacuum Science and Technology* **1981**, *19* (3), 456-462. DOI: <https://doi.org/10.1116/1.571038> (accessed 7/30/2025).

(24) Asaoka, Y. Desorption process of GaAs surface native oxide controlled by direct Ga-beam irradiation. *Journal of Crystal Growth* **2003**, *251* (1), 40-45. DOI: [https://doi.org/10.1016/S0022-0248\(02\)02492-2](https://doi.org/10.1016/S0022-0248(02)02492-2).

(25) Derriche, N.; Godin, S.; Greenwood, R.; Mercado, A.; Warner, A. N. Reflection High-Energy Electron Diffraction. *Energy* **2019**, *8* (100keV), 10-100eV.

(26) Diep, N. Q.; Tran, Q. T.; Huynh, T. B. T.; Wen, H. C.; Chou, W. C.; Huynh, S. H.; Le, V. Q.; Chu, Y. H.; Vu, T. T. Growth Mode Transition in Two-Dimensional GaSe on Three-Dimensional GaN/Sapphire Platform: Implication for Self-Powered Photodetection. *ACS Applied Nano Materials* **2024**. DOI: <https://doi.org/10.1021/acsanm.3c05343>.

(27) Liu, C.-W.; Dai, J.-J.; Wu, S.-K.; Diep, N.-Q.; Huynh, S.-H.; Mai, T.-T.; Wen, H.-C.; Yuan, C.-T.; Chou, W.-C.; Shen, J.-L.; et al. Substrate-induced strain in 2D layered GaSe materials grown by molecular beam epitaxy. *Scientific Reports* **2020**, *10* (1), 12972. DOI: <https://doi.org/10.1038/s41598-020-69946-4>.

(28) Hoff, R. M.; Irwin, J. C. Resonant Raman scattering in GaSe. *Physical Review B* **1974**, *10* (8), 3464-3470. DOI: <https://doi.org/10.1103/PhysRevB.10.3464>.

(29) Irwin, J. C.; Hoff, R. M.; Clayman, B. P.; Bromley, R. A. Long wavelength lattice vibrations in GaS and GaSe. *Solid State Communications* **1973**, *13* (9), 1531-1536. DOI: [https://doi.org/10.1016/0038-1098\(73\)90205-6](https://doi.org/10.1016/0038-1098(73)90205-6).

(30) Oda, H.; Inoue, K.; Ikeda, N.; Sugimoto, Y.; Asakawa, K. Observation of Raman scattering in GaAs photonic-crystal slab waveguides. *Optics Express* **2006**, *14* (15), 6659. DOI: <https://doi.org/10.1364/oe.14.006659> (accessed 2025-11-14T18:38:31).

(31) Cuscó, R.; Alarcón-Lladó, E.; Artús, L.; Hurst, W. S.; Maslar, J. E. Raman scattering by LO-phonon--plasmon coupled modes in  $\text{Ga}_{1-x}\text{In}_x\text{As}_y\text{Sb}_{1-y}$ : Role of Landau damping. *Physical Review B* **2010**, *81* (19), 195212. DOI: <https://doi.org/10.1103/PhysRevB.81.195212>.

(32) Rumaner, L.; Olmstead, M.; Ohuchi, F. Interaction of GaSe with GaAs(111): Formation of heterostructures with large lattice mismatch. *Journal of Vacuum Science & Technology B: Microelectronics and Nanometer Structures* **1998**, *16*. DOI: <https://doi.org/10.1116/1.590055>.

(33) Scimeca, T.; Watanabe, Y.; Berrigan, R.; Oshima, M. Surface chemical bonding of selenium-treated GaAs(111)A, (100), and (111)B. *Physical Review B* **1992**, *46* (16), 10201-10206. DOI: <https://doi.org/10.1103/PhysRevB.46.10201>.

(34) Wang, G.-C.; Lu, T.-M. RHEED Transmission Mode and Pole Figures. **2014**. DOI: <https://doi.org/10.1007/978-1-4614-9287-0>.

(35) Fan, X.; Zhao, Y.; Zheng, W.; Li, H.; Wu, X.; Hu, X.; Zhang, X.; Zhu, X.; Zhang, Q.; Wang, X.; et al. Controllable Growth and Formation Mechanisms of Dislocated WS<sub>2</sub> Spirals. *Nano Letters* **2018**, *18* (6), 3885-3892. DOI: <https://doi.org/10.1021/acs.nanolett.8b01210>.

(36) Seyhan, A.; Karabulut, O.; Akçinoğlu, B. G.; Aslan, B.; Turan, R. Optical anisotropy in GaSe. *Crystal Research and Technology* **2005**, *40* (9), 893-895. DOI: <https://doi.org/10.1002/crat.200410452> (accessed 2026/02/12).

(37) Arutyunyan, N. R.; Rybkovskiy, D. V.; Obraztsova, E. A.; Obraztsova, E. D. Size-induced evolution of optical properties in gallium selenide thin layers. *Journal of Luminescence* **2022**, *242*, 118546. DOI: <https://doi.org/10.1016/j.jlumin.2021.118546>.